Prismatic spreading-constriction expression for the improvement of impedance spectroscopy models and a more accurate determination of the internal thermal contact resistances of thermoelectric modules

Mutabe Aljaghtham[1], Ge Song[2], Jorge García-Cañadas[3], and Braulio Beltrán-Pitarch[4,*]

[1]*Department of Mechanical Engineering, Prince Sattam Bin Abdulaziz University, Al-Kharj 16278, Saudi Arabia*

[2]*College of Civil Engineering, Hunan University, Changsha, 4100182 Hunan, China*

[3]*Department of Industrial Systems Engineering and Design, Universitat Jaume I, Campus del Riu Sec, 12006 Castelló de la Plana, Spain*

[4]*DTU Energy – Department of Energy Conversion and Storage, Technical University of Denmark, Fysikvej 310, DK-2800 Kgs Lyngby, Denmark*

[*]*e-mail: brapit@dtu.dk*

ABSTRACT

Thermoelectric devices can convert heat to electrical power, or use electrical power to generate a temperature difference. Their characterization is essential to develop devices with higher efficiency. Impedance spectroscopy models have been developed in the last few years, and it has become a highly advantageous method for thermoelectric systems characterization. Recently, it has been shown that this technique can also be used to determine internal thermal contacts (between the thermoelectric legs and the metallic strips that connect them, and between the metallic strips and the outer layers). Here, we developed for the first time a spreading-constriction expression which does not assume cylindrical geometry. The enhanced model is also used to characterize four thermoelectric devices from different manufacturers, highlighting overestimations up to 13% when the previous cylindrical approximation is used. A code is provided in the Supporting Information ready to fit experimental data. This study positions impedance spectroscopy as a powerful tool to detect and monitor issues during manufacturing or operation of thermoelectric devices, which typically occur at the contacts.

Keywords: Peltier device, frequency domain, numerical simulations, finite element method, spreading-constriction, electrical impedance spectroscopy

INTRODUCTION

Thermoelectric (TE) devices can convert heat into electricity via the Seebeck effect, or use electrical power to establish a temperature difference across the device and provide cooling (Peltier effect). This technology has been successfully in use for many years in aerospace missions and cooling applications,[1,2] and recently has gained attention for the power generation in other areas where heat is available, such as industries,[3,4] the human body,[5,6] combustion engines,[7–9] or even in volcanos.[10] TE systems have several advantages difficult to overcome by other technologies, for example, they are environmentally friendly, silent, compact, and have no moving parts (free of maintenance). However, low efficiency of current TE generators is limiting the applicability of this technology. To improve the efficiency of TE generators at a faster pace not only is necessary to solve coupled challenges in materials development and systems engineering,[11,12] but to modernize the characterization techniques of all the material properties and device parameters that affect the generator performance.[13]

One of the most interesting techniques for the characterization of TE systems is electrical impedance spectroscopy. Since the introduction of this technique a few years back,[14,15] a lot of progress has been made to develop this method.[16–22] Recently, it has been shown that impedance spectroscopy can also be used to determine internal thermal contacts,[23] which are very challenging to be measured by other techniques.[24] The impedance method was able to characterize both the thermal contacts, between TE legs and the metallic strips that connect the TE legs,[25] and between the metallic strips and the outer layers (typically ceramics).[26]

When determining the internal thermal contacts, it is key to accurately model the thermal phenomena that is influenced by the changes in area of the different materials of the TE module (typically, the area of the TE legs is lower than the metallic strips that connect them, and their area is lower than that of the outer ceramics). The spreading-constriction impedance is the main element that accounts for these changes in area. The first spreading-constriction impedance developed for TE devices assumed constant temperature at the outer ceramic surfaces, which is only true if the TE module is contacted with ideal heat exchangers without thermal contact resistance.[27] A second spreading-constriction impedance considered uniform heat flux at the same locations, which is only achieved in perfect adiabatic conditions.[20] More recently, a more general spreading-constriction impedance that considers the variation of the heat flux in the radial direction at the outer ceramic surfaces has been derived.[25] However, all these three expressions were obtained assuming cylindrical geometry.

Here, we develop and analyze the accuracy improvement of the impedance spectroscopy models thanks to the new spreading-constriction impedance element, which considers the actual prismatic shape of the TE legs. In addition, we provide in the Supporting Information a validation though numerical simulations using the finite element method (FEM). Four TE devices from different manufacturers were fitted with the new analytical expression, and the results were compared with the cylindrical approximation (previously reported). The MATLAB code used to perform these fittings is also provided in the Supporting Information to assist potential users of the method.

ANALYTICAL MODEL

The theoretical model assumed in this study consist of a TE leg of length L and cross-sectional area A contacted by two metallic strips of length L_M which are also in contact with two external ceramic layers of length L_C. The ratio between the area of the TE legs and the area of the metallic strips (η_M) and the ratio between the area of TE legs and ceramics (η), define the cross-sectional area of the metallic strips, A/η_M, and ceramics, A/η, respectively. A thermal contact resistivity between the TE legs and the metallic strips, r_{TC1}, and between the metallic strips and the ceramic layers, r_{TC2}, is included.

The total impedance function, Z, for this model is defined by,

$$Z = j\omega L_p + R_\Omega + \left[{Z_{WCT}}^{-1} + (R_{TC1} + Z_{TOT})^{-1}\right]^{-1}, \tag{1}$$

where j=(-1)$^{0.5}$ is the imaginary number, ω the angular frequency (ω=2πf, being f the frequency), R_Ω is the total ohmic resistance of the TE device, L_p is a parasitic inductance, and Z_{TOT} is takes the form,

$$\begin{aligned} Z_{TOT} = &\left[{Z_{Wa,M}}^{-1} + \left(R_{TC2} + Z_{S/C} + Z_{Wa}\right)^{-1}\right]^{-1} \\ &+ \left({Z_{WCT,M}}^{-1} + {Z_{C_{TC2}}}^{-1} + {Z_{S/C,M}}^{-1} + {Z_{WCT,C,M}}^{-1}\right)^{-1}. \end{aligned} \tag{2}$$

All the elements in eq. (1) and (2) are defined as,

$$Z_{WCT} = \frac{2NS^2T_{initial}L}{\lambda_{TE}A}\left(\frac{j\omega}{\omega_{TE}}\right)^{-0.5} tanh\left[\left(\frac{j\omega}{\omega_{TE}}\right)^{0.5}\right], \tag{3}$$

$$R_{TC1} = \frac{4NS^2T_{initial}r_{TC1}}{A}, \tag{4}$$

$$Z_{Wa,M} = \frac{4NS^2T_{initial}L_M\eta_M}{\lambda_M A}\left(\frac{j\omega}{\omega_M}\right)^{-0.5} coth\left[\left(\frac{j\omega}{\omega_M}\right)^{0.5}\right], \tag{5}$$

$$Z_{WCT,M} = \frac{4NS^2T_{initial}L_M\eta_M}{\lambda_M A}\left(\frac{j\omega}{\omega_M}\right)^{-0.5} tanh\left[\left(\frac{j\omega}{\omega_M}\right)^{0.5}\right], \tag{6}$$

$$R_{TC2} = \frac{4NS^2T_{initial}r_{TC2}\eta_M}{A}, \tag{7}$$

$$Z_{S/C} = \frac{4NS^2T_{initial}z_{s/c}\eta_M}{A}, \tag{8}$$

$$Z_{Wa} = \frac{4NS^2 T_{initial} L_C \eta}{\lambda_C A} \left(\frac{j\omega}{\omega_C}\right)^{-0.5} coth\left[\left(\frac{j\omega}{\omega_C}\right)^{0.5}\right], \tag{9}$$

$$Z_{C_{TC2}} = \frac{4NS^2 T_{initial} {L_M}^2 \eta_M}{{\lambda_M}^2 A r_{TC2}} \left(\frac{j\omega}{\omega_M}\right)^{-1}, \tag{10}$$

$$Z_{S/C,M} = \frac{4NS^2 T_{initial} {L_M}^2 \eta_M}{{\lambda_M}^2 A z_{s/c}} \left(\frac{j\omega}{\omega_M}\right)^{-1}, \tag{11}$$

$$Z_{WCT,C,M} = \frac{4NS^2 T_{initial} {L_M}^2 \lambda_C \omega_M {\eta_M}^2}{{\lambda_M}^2 A L_C \eta \omega_C} \left(\frac{j\omega}{\omega_C}\right)^{-0.5} tanh\left[\left(\frac{j\omega}{\omega_C}\right)^{0.5}\right], \tag{12}$$

where $T_{initial}$ is the initial temperature, N is the number of TE couples, and S is the average Seebeck coefficient of all the TE legs. The constants λ_i, and ω_i are the average thermal conductivity, and characteristic angular frequency of each material, respectively: TE legs [$i=TE$, $\omega_{TE}=\alpha_{TE}/(L/2)^2$], metallic strips ($i=M$, $\omega_M=\alpha_M/L_M^2$), and external layers ($i=C$, $\omega_C=\alpha_C/L_C^2$), where, α_i is the thermal diffusivity of the material i.

This impedance expression has already been developed in previous works[23,25,26] however, it always considered a cylindrical approximation, see Figure 1a. Notice that this approximation only affects the spreading-constriction impedance, $z_{s/c}$, found in eq. (8) and (11). Therefore, the spreading-constriction impedance for prismatic geometry (see Figure 1b) was developed (full derivations can be found in the Supporting Information), and takes the form,

$$\begin{aligned} z_{s/c} = {} & \frac{2x_2 y_1}{\lambda_C \pi^2 x_1 y_2} \sum_{n=1}^{\infty} \frac{sin^2(\alpha_n x_1)}{n^2 \gamma_n} \left[\frac{\gamma_n \lambda_C + h_3\, tanh(\gamma_n L_C)}{\gamma_n \lambda_C\, tanh(\gamma_n L_C) + h_3}\right] \\ & + \frac{2y_2 x_1}{\lambda_C \pi^2 y_1 x_2} \sum_{m=1}^{\infty} \frac{sin^2(\beta_m y_1)}{m^2 \gamma_m} \left[\frac{\gamma_m \lambda_C + h_3\, tanh(\gamma_m L_C)}{\gamma_m \lambda_C\, tanh(\gamma_m L_C) + h_3}\right] \\ & + \frac{4x_2 y_2}{\lambda_C \pi^4 x_1 y_1} \sum_{n,m=1}^{\infty} \frac{sin^2(\alpha_n x_1)\, sin^2(\beta_m y_1)}{n^2 m^2 \gamma_{n,m}} \left[\frac{\gamma_{n,m} \lambda_C + h_3\, tanh(\gamma_{n,m} L_C)}{\gamma_{n,m} \lambda_C\, tanh(\gamma_{n,m} L_C) + h_3}\right] \end{aligned} \tag{13}$$

where h_3 is the convection coefficient at the outer ceramic surfaces (in this case h_3=0 because all measurements were performed in vacuum). The constants $\alpha_n=n\pi/x_2$, $\beta_m=m\pi/y_2$, $\gamma_n=(\alpha_n^2+j\omega/\alpha_C)^{1/2}$,$\gamma_m=(\beta_m^2+j\omega/\alpha_C)^{1/2}$, and $\gamma_{n,m}=(\alpha_n^2+\beta_m^2+j\omega/\alpha_C)^{1/2}$ define all the possible solutions for the values n and m. The geometrical parameters $x_1=(A/\eta)^{1/2}/2+A^{1/2}/2$, $x_2=(A/\eta)^{1/2}$, $y_1=A^{1/2}/2$, and $y_2=(A/\eta)^{1/2}/2$, are shown in Fig. S1 of the Supporting Information.

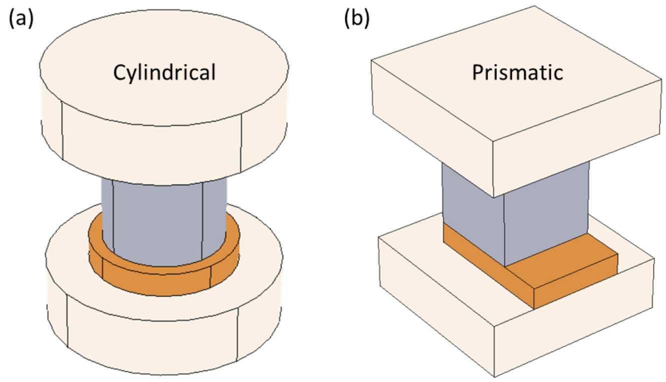

Figure 1. Schematic of (a) the geometry used in previous works, and (b) the geometry created in this work. All models consist of five layers where the color represents the material: thermoelectric leg (grey), metal (orange), and ceramic (cream).

EXPERIMENTAL SETUP

Four TE devices from different manufacturers were measured: Module 1 (Custom Thermoelectric, ref. 04801-933B-34RB), Module 2 (Interm, ref. CBM-88), Module 3 (European Thermodynamics, ref. 693–7080), and Module 4 (Jeongkwan Co. Ltd.). The specifications of these modules can be found in Table 1. Notice that the specifications of Module 3 were used for the numerical validation using COMSOL Multiphysics provided in the Supporting Information.[28]

Table 1. Specifications of the four TE devices evaluated in this study.

Name	Size (mm^2)	N	L (mm)	L_M (mm)	L_C (mm)	A (mm^2)	η_M	η
Module 1	10×10	48	0.55	0.03	0.525	0.6×0.6	0.71	0.35
Module 2	14×14	39	1.1	0.06	0.5	0.6×0.6	0.50	0.14
Module 3	40×40	127	1.2	0.3	0.75	1.3×1.3	0.67	0.27
Module 4	40×40	127	1.6	0.2	1.0	1.73×1.73	0.87	0.48

All measurements were performed in vacuum (<5x10^{-4} mbar) with the TE modules suspended by their wires and at room temperature. A commercial PGSTAT302N potentiostat (Metrohm Autolab B. V.) equipped with a FRA32M impedance module was connected to the wires of the TE modules using crocodile clamps. The potentiostat was controlled by Nova 1.11 software, which directly provides the impedance spectra. A current amplitude I_{ac}=30 mA was used for all four TE modules after a basic optimization.[29] This optimization consists in performing a few measurements at different current amplitudes, and choosing a current value just high enough to obtain the spectra free of noise. A logarithmically distributed frequency range of 50 measuring points from 10 mHz to 1 MHz was chosen for all measurements to ensure enough points in the high frequency part.

RESULTS AND DISCUSSION

Figure 2 shows the experimental impedance spectra of the four TE modules studied (dots) and their fittings (lines) using the MATLAB code provided in the Supporting Information. This code derives from ref.[25] but it includes the new expression for the spreading-constriction impedance. It should be noted that a few points at the highest frequencies (4 points for Module 1 and Module 2, and 6 points for Module 3 and Module 4) were not included in the fittings since they deviate from a purely inductive behavior. Following the procedure explained in ref.[25], L_p, R_Ω, r_{TC1}, λ_{TE}, and λ_C were fitted, maintaining fixed as constant values α_{TE}=0.37 mm^{2}s^{-1}, α_C=10 mm^{2}s^{-1}, λ_M=400 Wm^{-1}K^{-1}, and α_M=110 mm^{2}s^{-1}. The Seebeck coefficient of these modules were also fixed to the previously measured values (222.24 µVK^{-1}, 193.65 µVK^{-1}, 191.72 µVK^{-1}, and 190.08 µVK^{-1} for Module 1, Module 2, Module 3, and Module 4, respectively).[25,26] The fitted values (obtained from the MATLAB function lsqnonlin) with their relative errors (estimated from the variance-covariance matrix) can be found in Table 2. In all four TE modules, the parasitic inductance appears at the highest frequencies, and must be included in the fittings. However, all fittings converged nicely, which indicates that this unwanted parameter is not affecting the fitted values significantly.

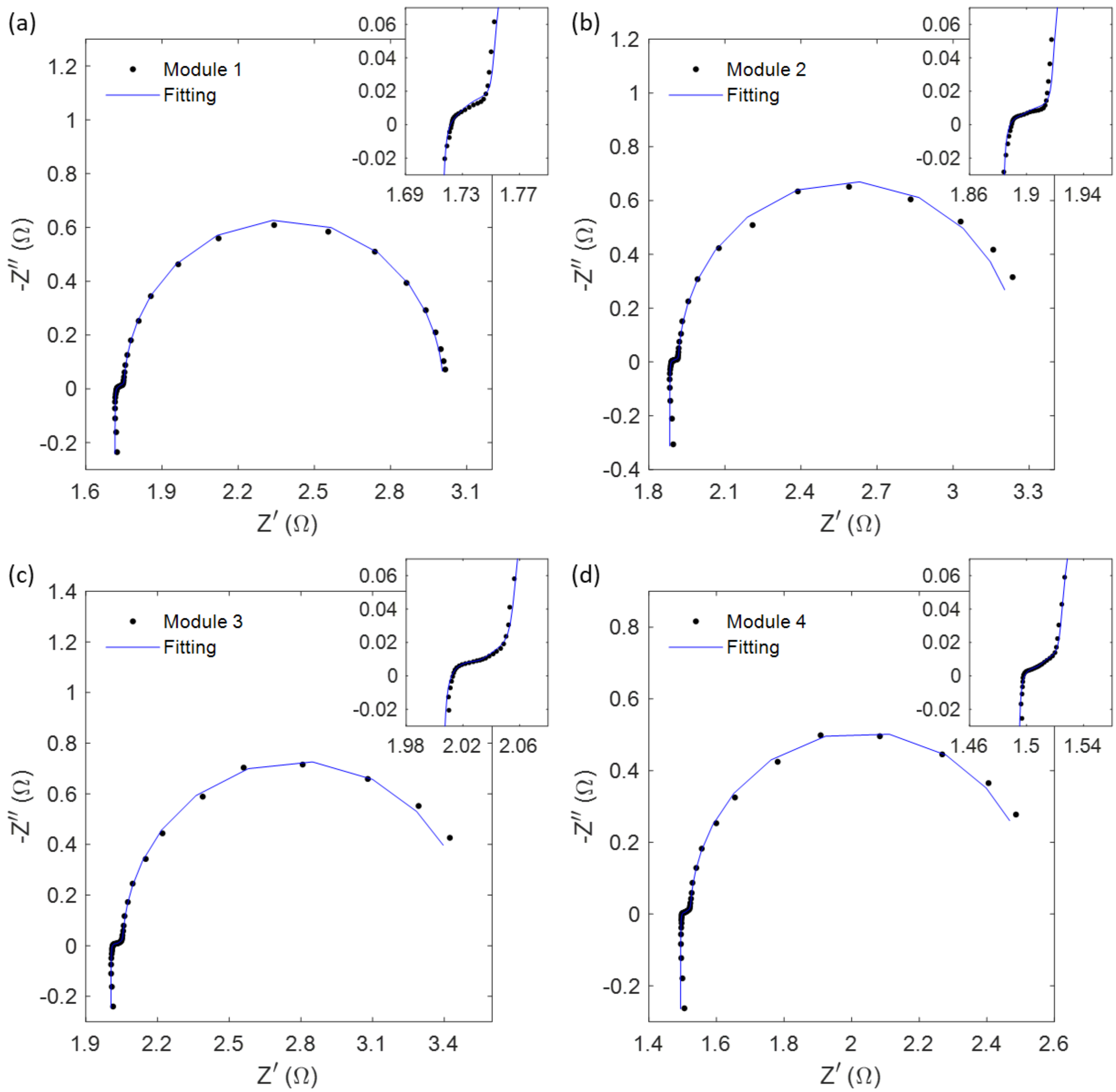

Figure 2. Experimental Nyquist plots impedance spectroscopy measurements (black dots) and their fittings (blue lines) using the MATLAB code provided in the Supporting Information for (a) Module 1, (b) Module 2, (c) Module 3, and (d) Module 4. *Z'* refers to the real part of the impedance, while *Z''* refers to the imaginary. The insets show a magnification of the high frequency part of the impedance spectra.

The four TE modules used in this study were previously fitted with the cylindrical approximation, showing similar values of L_p, R_Ω, λ_{TE}, and λ_C.[25,26] However, the previous fitted values of r_{TC1} were 13%, 10%, 4%, and 1% larger for Module 1, Module 2, Module 3, and Module 4, respectively (see last three columns of Table 2). Notice that the 4% overestimation in r_{TC1} for Module 3 is validated by the numerical simulations provided in the Supporting Information. Although it can be seen that all four TE modules produced a larger value of r_{TC1} when fitted with the cylindrical approximation, their overestimations were significantly different (varying from 1% to 13%). The reason behind this difference is not straightforward since the impedance spectra depends on many parameters, which makes difficult to know when the cylindrical approximation can be used. Since TE modules with larger filling factor are less affected by spreading-constriction effects (lower area change), it is not surprising that Module 4 showed the lowest deviation, followed by Module 3, and Module 2 (see Table 1). The highest deviation, however, was obtained for Module 1, which has a filling factor similar to Module 3. A possible explanation could be that the lower length of the TE legs of Module 1 increases the influence of the spreading-constriction impedance when performing fittings, since a lower leg length produces a more complete closing of the semicircle of the impedance spectrum at lower frequencies (right part of Figure 2a).

Table 2. Fitting parameters and their relative errors (in brackets) of the four TE devices measured in this study. All the fittings were performed using the MATLAB code provided in the Supporting Information. The last two columns show the values of r_{TC1} previously obtained with the cylindrical approximation,[25,26] and their overestimation.

Name	L_p (H)	R_Ω (Ω)	λ_{TE} (Wm^{-1}K^{-1})	λ_C (Wm^{-1}K^{-1})	r_{TC1} (m^{2}KW^{-1})	Previous r_{TC1} (m^{2}KW^{-1})	Deviation in r_{TC1}
Module 1	1.74×10^{-7} (1.05 %)	1.71 (0.030 %)	1.68 (0.28 %)	29.48 (0.58 %)	1.94×10^{-6} (6.72 %)	2.20×10^{-6} (5.89 %)	13.4 %
Module 2	2.24×10^{-7} (2.30 %)	1.88 (0.044 %)	1.95 (0.81 %)	28.11 (1.19 %)	4.83×10^{-6} (7.76 %)	5.29×10^{-6} (7.19 %)	9.5 %
Module 3	3.74×10^{-7} (2.51 %)	2.00 (0.038 %)	1.32 (0.84 %)	27.59 (1.01 %)	1.21×10^{-5} (4.35 %)	1.26×10^{-5} (4.33 %)	4.1 %
Module 4	4.06×10^{-7} (1.79 %)	1.49 (0.037 %)	1.41 (0.79 %)	27.07 (1.11 %)	1.16×10^{-5} (6.33 %)	1.17×10^{-5} (6.37 %)	0.9 %

CONCLUSIONS

A new impedance spectroscopy analytical expression was developed, which considers for the first time the actual prismatic shape of the thermoelectric legs of commercial thermoelectric modules. This was achieved by deriving a new spreading-constriction impedance element. Four thermoelectric modules from different manufacturers were fitted with the new analytical expression, and the results were compared with a previous characterization using the cylindrical approximation. The experiments revealed overestimations in the thermal contact resistances between the thermoelectric legs and the metallic strips that connect them of up to 13% when the previous cylindrical approximation is used. A numerical validation is provided in the Supporting Information. The MATLAB code used to perform the fittings is also available in the Supporting Information. This study significantly improves the accuracy of current impedance spectroscopy models for internal thermal contacts determination, and increases the potential of this method to be used as a tool to detect and monitor issues during manufacturing or operation of thermoelectric devices.

DATA AVAILABILITY

The data that support the findings of this study are available from the corresponding author upon request.

SUPPORTING INFORMATION

The derivations to obtain the spreading-constriction impedance, and a numerical validation of the new impedance expression is available as Supporting Information. The MATLAB code used to perform the fittings in this manuscript is also provided.

ACNOWLEDGMENTS

The authors acknowledge the companies European Thermodynamics Ltd. and Jeongkwan Co. Ltd. for supplying thermoelectric devices. Financial support from the Universitat Jaume I under the project number UJI-B2019-50 is also acknowledged.

REFERENCES

(1) M. Atta, R. Thermoelectric Cooling; Arangures, P., Ed.; IntechOpen, 2018. https://doi.org/10.5772/intechopen.75791.

(2) Zhao, D.; Tan, G. A Review of Thermoelectric Cooling : Materials , Modeling and Applications. *Appl. Therm. Eng.* **2014**, *66* (1–2), 15–24. https://doi.org/10.1016/j.applthermaleng.2014.01.074.

(3) Aneke, M.; Agnew, B.; Underwood, C.; Wu, H.; Masheiti, S. Power Generation from Waste Heat in a Food Processing Application. *Appl. Therm. Eng.* **2012**, *36* (1), 171–180. https://doi.org/10.1016/J.APPLTHERMALENG.2011.12.023.

(4) Wang, R. Q.; Jiang, L.; Wang, Y. D.; Roskilly, A. P. Energy Saving Technologies and Mass-Thermal Network Optimization for Decarbonized Iron and Steel Industry: A Review. *J. Clean. Prod.* **2020**, *274*, 122997. https://doi.org/10.1016/J.JCLEPRO.2020.122997.

(5) Sargolzaeiaval, Y.; Ramesh, V. P.; Ozturk, M. C. A Comprehensive Analytical Model for Thermoelectric Body Heat Harvesting Incorporating the Impact of Human Metabolism and Physical Activity. *Appl. Energy* **2022**, *324*, 119738. https://doi.org/10.1016/J.APENERGY.2022.119738.

(6) Siddique, A. R. M.; Mahmud, S.; Heyst, B. Van. A Review of the State of the Science on Wearable Thermoelectric Power Generators (TEGs) and Their Existing Challenges. *Renewable and Sustainable Energy Reviews*. 2017. https://doi.org/10.1016/j.rser.2017.01.177.

(7) Aljaghtham, M.; Celik, E. Design Optimization of Oil Pan Thermoelectric Generator to Recover Waste Heat from Internal Combustion Engines. *Energy* **2020**, *200*, 117547. https://doi.org/10.1016/J.ENERGY.2020.117547.

(8) Massaguer, A.; Pujol, T.; Comamala, M.; Massaguer, E. Feasibility Study on a Vehicular Thermoelectric Generator Coupled to an Exhaust Gas Heater to Improve Aftertreatment's Efficiency in Cold-Starts. *Appl. Therm. Eng.* **2020**, *167*, 114702. https://doi.org/10.1016/J.APPLTHERMALENG.2019.114702.

(9) Burnete, N. V.; Mariasiu, F.; Depcik, C.; Barabas, I.; Moldovanu, D. Review of Thermoelectric Generation for Internal Combustion Engine Waste Heat Recovery. *Prog. Energy Combust. Sci.* **2022**, *91*, 101009. https://doi.org/10.1016/J.PECS.2022.101009.

(10) Catalan, L.; Garacochea, A.; Casi, A.; Araiz, M.; Aranguren, P.; Astrain, D. Experimental Evidence of the Viability of Thermoelectric Generators to Power Volcanic Monitoring Stations. *Sensors* **2020**, *20* (17), 4839. https://doi.org/10.3390/S20174839.

(11) LeBlanc, S. Thermoelectric Generators: Linking Material Properties and Systems Engineering for Waste Heat Recovery Applications. *Sustain. Mater. Technol.* **2014**, *1*, 26–35. https://doi.org/10.1016/j.susmat.2014.11.002.

(12) Aljaghtham, M.; Celik, E. Design of Cascade Thermoelectric Generation Systems with Improved Thermal Reliability. *Energy* **2022**, *243*, 123032. https://doi.org/10.1016/J.ENERGY.2021.123032.

(13) Zhang, Q. H.; Huang, X. Y.; Bai, S. Q.; Shi, X.; Uher, C.; Chen, L. D. Thermoelectric Devices for Power Generation: Recent Progress and Future Challenges. *Advanced Engineering Materials*. Wiley-VCH Verlag February 1, 2016, pp 194–213. https://doi.org/10.1002/adem.201500333.

(14) Dilhaire, S.; Patino-Lopez, L. D.; Grauby, S.; Rampnoux, J. M.; Jorez, S.; Claeys, W. Determination of ZT of PN Thermoelectric Couples by AC Electrical Measurement. In *International Conference on Thermoelectrics, ICT, Proceedings*; Institute of Electrical and Electronics Engineers Inc., 2002; Vol. 2002-Janua, pp 321–324. https://doi.org/10.1109/ICT.2002.1190330.

(15) Downey, A. D.; Hogan, T. P.; Cook, B. Characterization of Thermoelectric Elements and Devices by Impedance Spectroscopy. *Rev. Sci. Instrum.* **2007**, *78* (9), 093904. https://doi.org/10.1063/1.2775432.

(16) De Marchi, A.; Giaretto, V.; Caron, S.; Tona, A. A Novel ZT Meter Based on the Porcupine Method and a Survey on the Size of the Snout Correction Needed for Various Thermoelectric Devices. *J. Electron. Mater.* **2013**, *42* (7), 2067–2072. https://doi.org/10.1007/s11664-013-2530-2.

(17) García-cañadas, J.; Min, G. Impedance Spectroscopy Models for the Complete Characterization of Thermoelectric Materials. *J. Appl. Phys.* **2014**, *116*, 174510. https://doi.org/10.1063/1.4901213.

(18) Hasegawa, Y.; Homma, R.; Ohtsuka, M. Thermoelectric Module Performance Estimation Based on Impedance Spectroscopy. *J. Electron. Mater.* **2016**, *45* (3), 1886–1893. https://doi.org/10.1007/s11664-015-4271-x.

(19) Beltrán-Pitarch, B.; García-Cañadas, J. Influence of Convection at Outer Ceramic Surfaces on the Characterization of Thermoelectric Modules by Impedance Spectroscopy. *J. Appl. Phys.* **2018**, *123* (8), 084505. https://doi.org/10.1063/1.5019881.

(20) Mesalam, R.; Williams, H. R.; Ambrosi, R. M.; García-Cañadas, J.; Stephenson, K. Towards a Comprehensive Model for Characterising and Assessing Thermoelectric Modules by Impedance Spectroscopy. *Appl. Energy* **2018**, *226*, 1208–1218. https://doi.org/10.1016/j.apenergy.2018.05.041.

(21) Yoo, C.-Y.; Yeon, C.; Jin, Y.; Kim, Y.; Song, J.; Yoon, H.; Park, S. H.; Beltrán-Pitarch, B.; García-Cañadas, J.; Min, G. Determination of the Thermoelectric Properties of a Skutterudite-Based Device at Practical Operating Temperatures by Impedance Spectroscopy. *Appl. Energy* **2019**, *251*, 113341. https://doi.org/10.1016/J.APENERGY.2019.113341.

(22) Beltrán-Pitarch, B.; Vidan, F.; García-Cañadas, J. Characterization of Thermal Contacts between Heat Exchangers and a Thermoelectric Module by Impedance Spectroscopy. *Appl. Therm. Eng.* **2019**, *165*, 114361. https://doi.org/10.1016/j.applthermaleng.2019.114361.

(23) Beltrán-Pitarch, B. Advanced Characterization of Thermoelectric Materials and Devices by Impedance Spectroscopy, Universitat Jaume I, Castelló, 2020. https://doi.org/10.6035/14107.2020.428227.

(24) Min, G.; Phillips, M. Preparation and Characterization of TE Interfaces/Junctions; John Wiley & Sons, Ltd, 2017; pp 111–125. https://doi.org/10.1002/9783527698110.ch6.

(25) Beltrán-Pitarch, B.; Maassen, J.; García-Cañadas, J. Comprehensive Impedance Spectroscopy Equivalent Circuit of a Thermoelectric Device Which Includes the Internal Thermal Contact Resistances. *Appl. Energy* **2021**, *299* (June), 117287. https://doi.org/10.1016/j.apenergy.2021.117287.

(26) Beltrán-Pitarch, B.; García-Cañadas, J. Impedance Spectroscopy Analysis of Thermoelectric Modules Fabricated with Metallic Outer External Layers. *ACS Appl. Electron. Mater.* **2021**. https://doi.org/10.1021/acsaelm.1c00670.

(27) Casalegno, F.; De Marchi, A.; Giaretto, V. Frequency Domain Analysis of Spreading-Constriction Thermal Impedance. *Rev. Sci. Instrum.* **2013**, *84* (2), 024901. https://doi.org/10.1063/1.4789765.

(28) COMSOL AB. COMSOL Multiphysics®. www.comsol.com: Stockholm, Sweden.

(29) Beltrán-Pitarch, B.; Prado-Gonjal, J.; Powell, A. V.; García-Cañadas, J. Experimental Conditions Required for Accurate Measurements of Electrical Resistivity, Thermal Conductivity, and Dimensionless Figure of Merit (ZT) Using Harman and Impedance Spectroscopy Methods. *J. Appl. Phys.* **2019**, *125*, 025111. https://doi.org/10.1063/1.5077071.

(30) Muzychka, Y.; Culham, R.; Yovanovich, M. Thermal Spreading Resistances in Rectangular Flux Channels: Part I Geometric Equivalences. In *36th AIAA Thermophysics Conference*; Reston, Virigina, 2003. https://doi.org/10.2514/6.2003-4187.

For Table of Contents Use Only.